ELSEVIER

Real-time two-dimensional terahertz tomography of moving objects

Takashi Yasuda [a], Takeshi Yasui [a,*], Tsutomu Araki [a], Emmanuel Abraham [b]

[a] *Graduate School of Engineering Science, Osaka University, 1–3 Machikaneyama-cho, Toyonaka, Osaka 560-8531, Japan*
[b] *Centre de Physique Moléculaire, Optique et Hertzienne, UMR5798, Université Bordeaux I, 351, Cours de la Libération, 33405 Talence, France*

Abstract

We propose real-time two-dimensional (2D) terahertz (THz) tomography for 2D cross-sectional imaging of moving objects. The proposed method does not require mechanical scanning elements for time delay and sample position, which are essential for conventional THz tomography. For this purpose, a 2D spatiotemporal THz image is acquired at a frame rate of 10 frame/s by a combination of time-to-space conversion using non-collinear 2D free-space electro-optic sampling and line focusing of a THz beam on a sample. We demonstrate the use of real-time 2D THz tomography for real-time monitoring of the paint thickness in a moving paint sample and the drying progress in a wet paint film. The proposed method provides a powerful tool for non-ionizing and non-contact probing in the fields of nondestructive testing and biomedical diagnostics.
© 2006 Elsevier B.V. All rights reserved.

1. Introduction

In fields of nondestructive testing and evaluation, it is important to visualize internal structures of an object as a cross-sectional image. Although X-rays and ultrasonic waves have been utilized for this purpose in industrial and biomedical applications, ionizing effect harmful to human health in the former and contact measurement in the latter limit certain applications. Terahertz (THz) tomography [1,2] has recently attracted attention as a possible substitute for these conventional methods because it can serve as a non-ionizing and non-contact probe. THz tomography is realized by the time-of-flight measurement of THz pulse echoes when a THz electromagnetic pulse is incident upon a sample in a reflection geometry. This technique can be used in various applications to reveal the cross-section of internal structures from the distribution of the group refractive index in samples. For example, the THz tomography clearly visualizes the 2D cross-section of tablet coating thickness, which is important to control the release of active pharmaceutical ingredients [3]. In the

skin diagnosis, a skin cancer area was recognized as a temporal distortion of the THz pulse echo signal [4]. Another application of THz tomography is in thickness measurement of the paint film of industrial products such as car bodies. Since conventional thickness meters, including ultrasonic testing, eddy-current testing, and electromagnetic testing, are based on contact measurement, it is difficult to apply for moving objects or wet paint films. One possible method for non-contact and remote measurement is optical coherence tomography [5]. However, colored paint film is usually opaque and causes strong scattering of visible and infrared light, resulting in decreased reliability of the measurement and low penetration depth [6]. Although a photothermal method [7] is suitable for thickness determination of the opaque painting film, this method is based on a point-to-point measurement, resulting in high time consuming to construct cross-section image of the object. We have previously proposed a THz paintmeter as a tool for testing paint films, and have successfully applied it for determination of painting thickness and its distribution in various kinds of paint films that can be hardly measured by conventional methods (for example, wet, metallic, paint-off, or multilayer paint film) [6]. Furthermore, the monitoring of dryness in a wet paint film

* Corresponding author. Tel.: +81 668506217; fax: +81 668506213.
  E-mail address: t-yasui@me.es.osaka-u.ac.jp (T. Yasui).

has been demonstrated by taking advantage of a distinct spectroscopic difference in the THz region between the wet and dry condition of a paint film. However, since usual THz tomography is also based on a point-to-point measurement, it is necessary to perform 2D mechanical scanning of the time delay and sample position to construct a 2D tomographic image of the sample. The resultant high time consumption of this method has limited its application to stationary objects. If THz tomography can be extended to moving objects, such as industrial products on a moving stage or the human body, the fields that THz tomography can be applied to will be greatly increased. For this, real-time image acquisition is essential.

Rapid image acquisition can be achieved if instead of a mechanical stage we use an alternative technique for measuring the time delay and sample position. One effective method to realize a stage-free configuration is a combination of a single-shot measurement of the temporal waveform and its one-dimensional (1D) transverse imaging, enabling real-time 2D spatiotemporal imaging. Such real-time 2D spatiotemporal imaging technique has been proposed in optical region and effectively applied to high-speed optical echography of biological tissues [8]. On the other hand, in THz region, there are a few reports on single-shot temporal measurement of THz pulses requiring no mechanical stage for time delay. These techniques are based on two-dimensional (2D) free-space electro-optic sampling (2D-FSEOS) [9]. By combining a linearly chirped optical probe pulse and a multi-channel spectrometer, the temporal waveform of a THz pulse can be converted into the wavelength spectrum of an optical probe pulse [10]. Such a time-to-wavelength conversion method can be applied to 2D spatiotemporal THz imaging [11]. However, the time resolution in this method is limited by a tradeoff inherent in combining frequency and time domain methods [12], though this limitation can be overcome by the non-collinear cross-correlation of electro-optic (EO) modulated optical pulses, requiring a more complicated optical setup [13]. One possible method for single-shot measurement of

THz waveforms is the use of a long probe pulse and a streak camera [14]. In this method, the temporal profile of the EO modulated probe pulse is transformed into the spatial distribution of the probe light intensity through time-to-space conversion in a streak tube and is then detected with a 2D charge-coupled-device (CCD) camera. Although this method may be also extended to 2D spatio-temporal THz imaging, the time resolution of this method is limited by the response of the streak camera, typically from subpicosecond to picosecond. Furthermore, this single-shot measurement method needs expensive and complicated streak camera. Another possible method is the use of 2D-FSEOS with the THz beam and optical probe pulse in a non-collinear geometry (non-collinear 2D-FSEOS) [15]. In this geometry, direct time-to-space conversion occurs through the spatial overlap of the two non-collinear beams in an EO crystal and the resulting spatial distribution of the probe beam is detected with a 1D photodiode array. This method is easily achieved by a slight modification of a regular 2D-FSEOS system without any expensive apparatus or complicated setup, and most advantageously, it has no limitations on time resolution caused by the intrinsic coupling between frequency and time domain methods [12] or the instrumental response [14]. Despite the simple configuration, suitable for 2D spatiotemporal THz imaging, there are no reports of its demonstration and hence no reported applications of real-time 2D THz tomography.

In this paper, we propose real-time 2D THz tomography by the combined use of non-collinear 2D-FSEOS and line focusing of the THz beam onto a sample coupled with a CCD camera. After describing the principle and experimental setup of the proposed method, we present THz tomographic images of a moving paint film and the drying progress of a wet paint film.

2. Principle and experimental setup

Fig. 1(a) shows the principle of non-collinear 2D-FSEOS [15]. Here, we consider a pulsed THz electric field
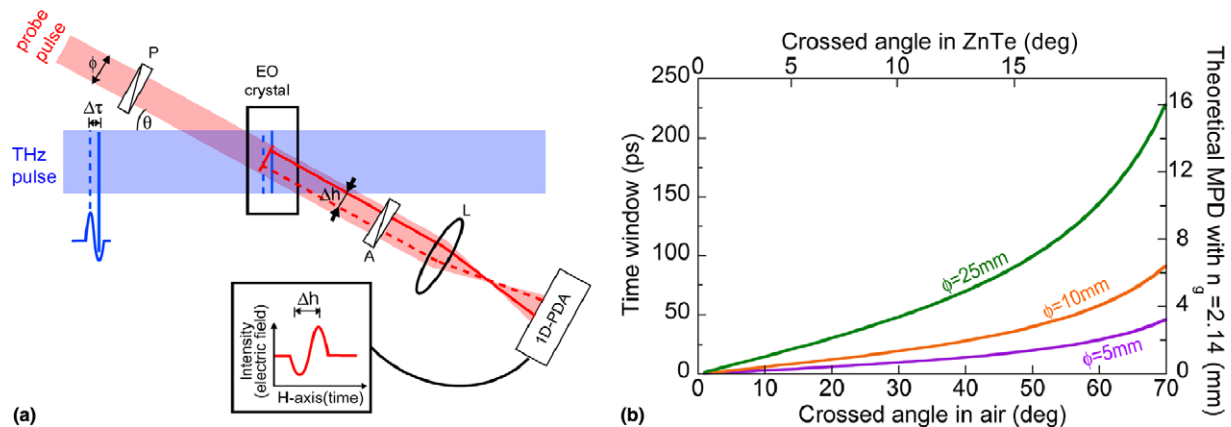

Fig. 1. (a) Principle of non-collinear 2D-FSEOS. P: polarizer; EO crystal: electro-optic crystal; A: analyzer; L: lens; 1D-PDA: one-dimensional photodiode array. Pulsed THz electric field is composed of a negative and a positive peak with a time delay of $\Delta\tau$. Δh is the spatial displacement transcribed from the time delay $\Delta\tau$. (b) Relationship between crossed angle and time window with respect to different probe beam diameters in non-collinear 2D-FSEOS. The right vertical axis is scaled for theortical maximum probing depth with group refractive index of 2.14.

to be composed of a negative and a positive peak with a time delay of $\Delta\tau$. The THz beam and the probe beam are non-collinearly incident on an EO crystal for FSEOS (for example, ZnTe crystal) at a crossed angle of θ in air. The two wavefronts of the negative and positive peaks of the THz beam (the solid and broken lines in Fig. 1(a)) overlap with the wavefront of the probe beam at different transverse positions of the probe beam. As a result of the non-collinear overlapping of the THz and probe beam wavefronts, the THz electric field at different times is translated into different positions across the transverse profile of the probe beam. To obtain the 1D spatial distribution, the EO modulated probe beam is detected with a 1D photodiode array (1D-PDA) using two perpendicular polarizers in a cross-Nicol configuration (P and A) and an imaging lens (L). The resultant time-to-space conversion factor is determined by

$$\Delta\tau = (\Delta h \cdot \tan\theta)/c \tag{1}$$

where Δh is the spatial displacement transcribed from the time delay $\Delta\tau$ and c is the velocity of light in vacuum. The temporal profile of the THz pulse can then be successively developed along the horizontal 1D-PDA. The measurable time window ΔT is defined as

$$\Delta T = (\phi \cdot \tan\theta)/c \tag{2}$$

where ϕ is the diameter of the probe beam. Fig. 1(b) shows the measurable time window ΔT with respect to different probe beam diameters ϕ in the case of ZnTe crystal, where the lower and upper horizontal coordinates are scaled as a crossed angle in air (θ) and that in the ZnTe (θ_i). From a

relationship of refractive indices between the ZnTe (=2.85 at 800 nm) and air (=1), the total reflection of the probe beam occurs at a back surface of the ZnTe when $\theta_i = 20.5°$ or $\theta = 90°$ (not shown in Fig. 1(b)). The maximum ϕ value ϕ_{max} is limited by the size of commercially available EO crystals. For example, $\phi_{max} = 75$ mm for the ZnTe crystal used in our experiment. The theoretical maximum probing depth (MPD) in THz tomography is determined by

$$\text{theoretical MPD} = (c\Delta T)/(2n_g) \tag{3}$$

where n_g is the group refractive index of the sample in THz region. The right vertical axis in Fig. 1(b) is scaled for *theoretical MPD* with $n_g = 2.14$ although the n_g value is a function of THz frequency. One can set *theoretical MPD* by the selection of θ and ϕ. However, *actual MPD* is limited by THz absorption in the sample and/or imaging performances in a THz optical system as discussed later.

To extend this non-collinear 2D-FSEOS to real-time 2D THz tomography, we prepared line focusing and imaging optics for the THz beam in a reflection configuration and a CCD camera, as shown in Fig. 2. A femtosecond Ti:sapphire regenerative amplifier (Spectra-Physics, Hurricane, pulse energy = 1 mJ, pulse duration = 100 fs, central wavelength = 800 nm, repetition rate = 1 kHz) was employed to generate and detect the THz pulse. An intense THz pulse is generated via optical rectification of amplified femtosecond pulse light (300-μJ pulse energy) in a 4-mm-thick $\langle 110 \rangle$ ZnTe crystal (ZnTe1). In the line focusing and imaging systems for the THz beam, we used three kinds of THz lenses manufactured by PAX, Ltd., Japan. The radiated THz
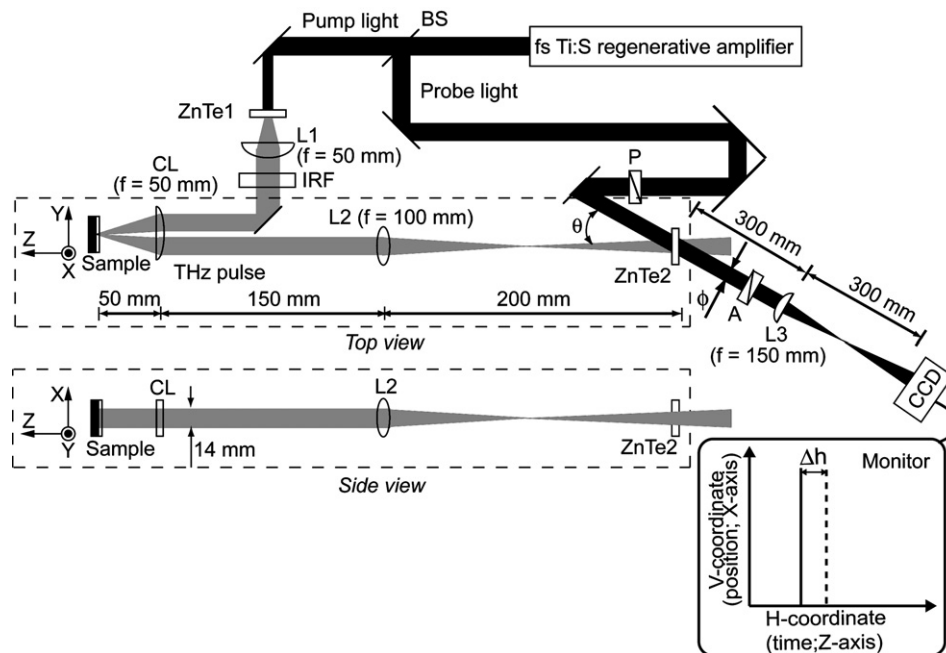

Fig. 2. Experimental setup of real-time 2D THz tomography. BS: beam splitter; ZnTe1 and ZnTe2: zinc telluride crystals; L1: plano-convex THz lens; IRF: infrared-cut filter; CL: cylindrical THz lens; L2: biconvex THz lens; P: polarizer; A: analyzer; L3: plano-convex lens; CCD: charge-coupled-device camera.

beam is collimated by a plano-convex THz lens (L1, $f = 50$ mm). A white polyethylene plate (IRF, thickness = 3 mm) was used as a filter to block the excess laser light passing through the ZnTe1. When the CCD camera is used as a detector for non-collinear 2 D-FSEOS, the spatial distribution Δh develops along the horizontal coordinate of the CCD camera, corresponding specifically to the time delay $\Delta \tau$ and hence the depth profile along the Z-axis of the sample (see Fig. 2). On the other hand, the vertical coordinate of the CCD camera can be used for one-dimensional (1D) transverse imaging of the sample along the X-axis. In Fig. 2, the top view and side view of the THz beam are illustrated to help in understanding the line focusing and imaging optics for the THz beam. To obtain a 1D transverse image along the X-axis of the sample, the THz beam is first line-focused on the sample using a cylindrical THz lens (CL, $f = 50$ mm) with the focal line parallel to the X-axis of the sample (see top and side views in Fig. 2), resulting in a line of 14-mm height being illuminated. Next, the line of the THz beam reflected from the sample is imaged by a biconvex THz lens (L2, $f = 100$ mm) onto a 1-mm-thick ⟨110⟩ ZnTe crystal for FSEOS (ZnTe2) (see side view in Fig. 2). A probe beam of 5-mm diameter (1-μJ pulse energy) is incident on the ZnTe2 non-collinearly with the THz beam at a crossed angle of θ. This results in the formation of a 2D spatiotemporal THz image on the probe beam at the exit window of the ZnTe2, in which the temporal profile of the THz pulse and its 1D transverse distribution along the X-axis develop in the horizontal and vertical directions in the ZnTe2. EO sampling is then performed at the near zero optical transmission point using two crossed polarizers (P and A, extinction ratio $= 5 \times 10^{-6}$) [16]. Finally, the 2D spatiotemporal THz image is imaged via a plano-convex lens (L3, $f = 150$ mm) onto a 12-bit thermoelectric-cooled CCD camera (PCO-imaging, SensiCam 360KL, 640×480 pixels, cooled to -15 °C, 10 frame/s at an exposure time of 70 ms and a readout time of 30 ms) as the 2D spatial distribution of the probe beam in real time. The resulting 2D spatiotemporal THz image provides an X–Z cross-sectional image of the sample, namely real-time 2D THz tomography.

Our proposed method has three attractive features. First, it is easily realized by a slight modification of conventional 2D-FSEOS, specifically a change from a collinear to a non-collinear configuration and the use of line focusing optics for the THz beam. Second, high-speed single-shot 2D THz tomography measurement is possible in principle. For example, if amplified femtosecond pulse light with a repetition rate of 1 kHz is used for THz generation and detection, a frame rate up to 1 kHz is possible [17]. Finally, and most importantly, this method can be applied to moving objects such as moving products on a belt conveyor or the human body.

3. Results

Fig. 3(a) shows a 2D spatiotemporal THz image of a single frame for a plane Al mirror surface at $\theta = 28°$ (image

size $= 9$ ps $\times$ 5 mm). The image was obtained by subtracting the CCD image measured in the absence of the THz electric field (background image) from the EO modulated image. The white and black areas in the image indicate positive and negative THz electric field, respectively. The time scale was calibrated from a known time delay produced by a conventional optical delay stage. The unit increment in the time axis was 14.1 fs/pixel, resulting from the time window of 9 ps and the horizontal width of 640 pixels. Fig. 3(b) shows a three-dimensional representation of the above 2D spatiotemporal THz image. The THz pulse echo reflected from the sample appears as a signal line around 4.1 ps (the vertical white line in Fig. 3(a)). This straight-line profile results from the uniform distribution of the mirror surface without internal structures. Fig. 3 (c) shows the temporal waveform of the THz electric field extracted from a line profile of the 2D spatiotemporal THz image (line (A) in Fig. 3(a)). As shown, a pulsed THz electric field with 0.5-ps pulse duration was obtained with a signal-to-noise ratio of 80. The time-resolution limitation of this method is mainly due to mismatching of the group velocity of the optical pulse with the phase velocity of the THz pulse along the THz propagation direction in the ZnTe2, which is discussed in detail elsewhere [15]. Fig. 3(d) shows an amplitude spectrum of the THz radiation obtained by Fourier transform of the temporal waveform in Fig. 3(c). The peak frequency and bandwidth of the spectrum are 0.55 THz and 1.04 THz, respectively. The dynamic range of the detection system is $S_D = 20\log(2^{12} - 508) = 71$ dB by taking into account 12-bit acquisition of the CCD camera and signal level of the background image (=(mean) $\pm$ (standard deviation) $= 508 \pm 166$), whereas a frame-to-frame variation of THz signal intensity was 0.3%.

Here, let us consider imaging performances of the present system. Performances of the line focusing and imaging systems of THz beam are summarized in Table 1, which are calculated using a peak frequency of THz amplitude spectrum (=0.55 THz; corresponding wavelength = 550 μm) and parameters of CL or L2. The width of THz focal line on a sample is 1.7 mm whereas the THz transverse resolution along the X direction of a sample (vertical coordinate in Fig. 3(a)) is 2.7 mm. From a viewpoint of applicability to an object with curved or stepped surface, we have to consider the depth of focus in THz line illumination and the depth of field in THz imaging. The depth of line focus and depth of field are estimated to be 14.3 mm and 43.7 mm in the present system, respectively. These values indicate that the proposed system is sufficiently allowable to a curved or stepped surface with an extreme roughness. Such allowance is attractive to apply this technique for industrial products on a moving stage even when an automatic focusing system of the THz beam is not employed. These values also indicate that the THz line focusing and imaging system well covers the theoretical MPD for $\phi = 5$ mm. We further have to consider effects of the ZnTe2 crystal thickness with respect to the depth of focus in the THz imaging system and the depth of field in the probe
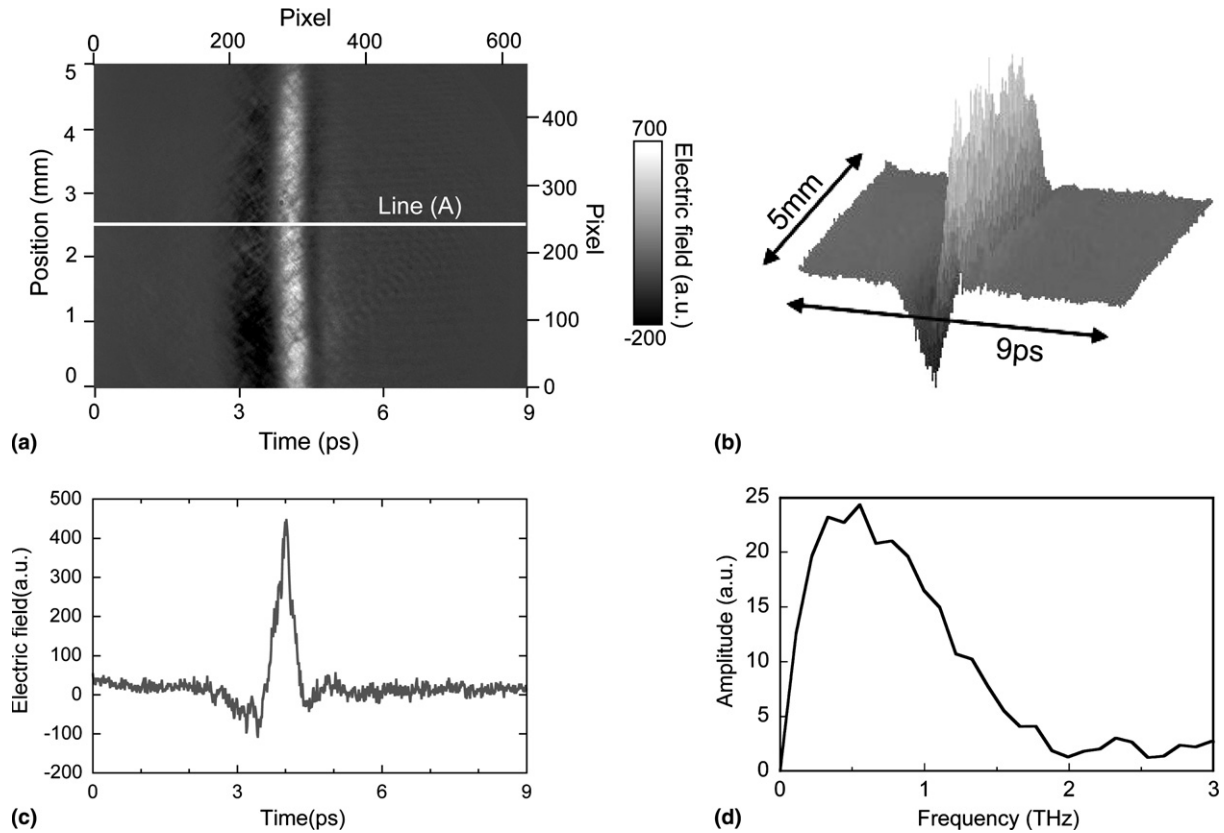
Fig. 3. 2D spatiotemporal THz image of a plane Al mirror surface ($\theta = 28°$, image size = 9 ps × 5 mm). (a) CCD image for an exposure time of 70 ms. The white and black areas in the image indicate positive and negative THz electric field, respectively. (b) 3D representation of the 2D spatiotemporal THz image. (c) Temporal waveform of the THz electric field extracted from a line profile of the 2D spatiotemporal THz image and (d) corresponding spectrum of THz amplitude.

Table 1
Imaging performances of THz and probe optical systems

	Transverse resolution	Depth of field	Depth of focus
THz beam			
Line focusing	1.7 mm		14.3 mm
Imaging	2.7 mm	43.7 mm	±21.6 mm
Probe beam			
Imaging	5.9 μm	150 mm	±71 μm

imaging system. Imaging performances of the probe beam passing through the ZnTe2 are also indicated in Table 1, which are calculated using a probe wavelength of 800 nm and parameters of L3. At the present setup, the focal depth of ±21.6 mm in THz imaging and the field depth of 150 mm in the probe imaging well cover the ZnTe2 thickness (=1 mm), resulting in no significant effect on the imaging characteristics. Another factor to degrade the spatial resolution is the spherical aberration induced by the refractive index mismatching between air and ZnTe crystal for THz beam and optical probe beam. Furthermore, the tilted surface of the ZnTe crystal to the probe beam may deteriorate the imaging characteristics in the probe imaging system. We consider that these effects limit the actual transverse resolution. To confirm it, we performed a knife-edge test in the present setup. The resulting trans-

verse resolution was 3.1 mm, which is dependent on frequency of THz amplitude spectrum (see Fig. 3(d)). A little difference between the theoretical and practical resolutions indicates that the above effects do not deteriorate the spatial resolution significantly.

Before performing real-time 2D THz tomography of paint films, we measured spectral characteristics of an oil, alkyd paint (white color; quick-drying type) with a THz time-domain spectroscopy [18], which is used as a sample in the following demonstrations. For this experiment, we prepared a dry paint film (thickness = 4.6 mm) and a wet one (thickness = 4.5 mm). The resulting spectra of absorption coefficient and phase refractive index are shown in Fig. 4(a) and (b). One can confirm that there are distinct differences in absorption coefficient and refractive index between the wet paint film and dry one. In general, the paint is composed of a resin (e.g., alkyd resin), a pigment and an organic solvent (e.g., paint thinner). The drying process of the paint is temporally advanced by the volatilization of the organic solvent. The volatilization helps the transformation to the dry condition. Therefore, such spectroscopic difference between them is mainly due to volatilization of the solvent and/or accompanying chemical change of the resin. For example, since the wet paint has the refractive index dominated by the solvent, the refractive
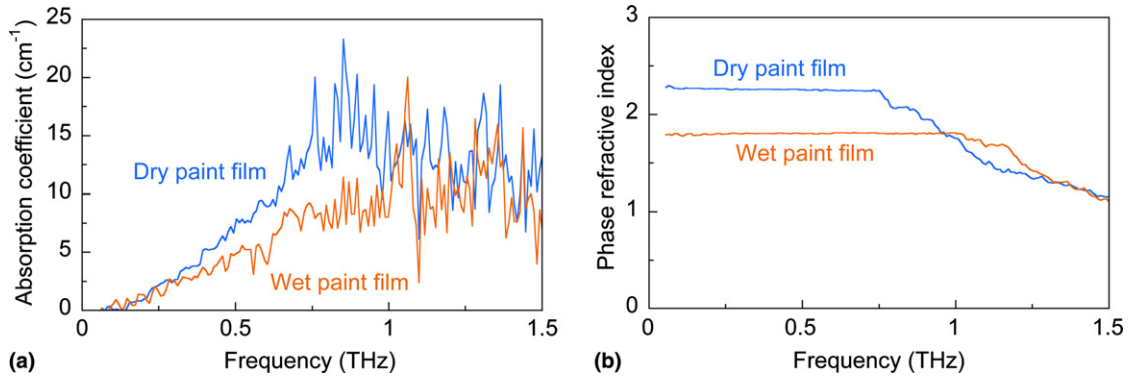
Fig. 4. Spectra of (a) absorption coefficient and (b) phase refractive index of oil, alkyd paint.

index of the wet paint film is smaller than that of the dry one and thus increases depending on drying degree. The spectral change accompanying the wet-to-dry transformation results in attenuation, delay, and/or distortion of the THz pulse echoes. With respect to the dry paint film, the THz pulse can reach to 2.9 mm in depth, which is calculated from absorption coefficient of 7.5 cm^{-1} at 0.55 THz (=spectral peak of THz radiation, see Fig. 3(d)) and a signal-to-noise ratio of 80 (see Fig. 3(c)). Also, we determined a typical n_g value of the dry paint film from a relationship between geometrical thickness measured with a contact-type thickness meter ($=d$) and optical thickness with a THz paintmeter ($=n_g d$) according to an analysis procedure in a previous paper [6] because the n_g value is a function of THz frequency. The resulting n_g value of the dry paint film was 2.14. Theoretical MPD in the present system is 0.42 mm for this paint from $n_g = 2.14$ and $\Delta T = 6$ ps ($\theta = 20°$ and $\phi = 5$ mm are used in the following demonstrations). From comparison of the penetration depth of 2.9 mm and theoretical MPD of 0.42 mm, the actual MPD in the present system is 0.42 mm. Further magnification of ΔT value and improvement of signal-to-noise ratio will lead to actual MPD more than several millimeters.

To confirm the performance of the proposed method, we have demonstrated real-time 2 D THz tomography of a moving paint film. The sample used in the experiment was a half-paint film, shown in Fig. 5, in which the dry white alkyd painting is layered on half the area of an Al substrate. The paint thickness around the center of the painting area was 175 µm, determined beforehand with the contact, eddy-current type thickness meter. Because the THz beam is line-focused on the sample (see top and side views in Fig. 2), the sample was continuously moved along the direction of the focus line (X direction in Figs. 2 and 5) by a translation stage (moving speed = 5 mm/s). A 2 D spatiotemporal THz movie, or 2D THz tomographic movie, of the moving half-paint film was measured at a frame rate of 10 frame/s when $\theta = 20°$ (see Movie 1). Fig. 5 illustrates snapshots of the movie at three different illuminating positions (image size = 6 ps × 5 mm), which provide 2D cross-sectional image of a sample. In the unpainted area, one THz echo line from the surface of the Al substrate appears at around 2.8 ps (Fig. 5(a)). In the painted area, two THz echo lines from the paint surface (2.3 ps) and the paint-substrate interface (4.5 ps) are clearly separated (Fig. 5(c)). Since the time separation between the
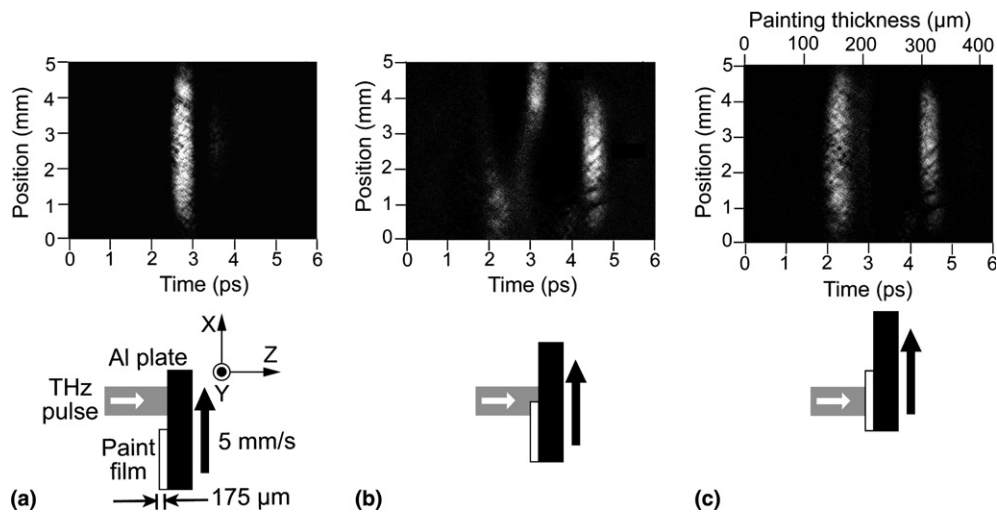

Fig. 5. 2D THz tomography at three different illuminating positions of the moving half-paint film ($\theta = 20°$, image size = 6 ps × 5 mm). (a) Unpainted area, (b) boundary between unpainted and painted areas, and (c) painted area.

two echoes corresponds to optical thickness of the paint film, the paint thickness can be determined using the group refractive index of the paint (2.14) and the time delay, as shown in the upper horizontal coordinate. Here, the thickness resolution (d_{min}) is determined from the duration of the THz pulse (Δt) and a group refractive index of a sample (n_g) as follows:

$$d_{min} = (c\Delta t)/(2n_g)$$
$$= (3 \times 10^8 \times 0.5 \times 10^{-12})/(2 \times 2.14) = 35 \text{ μm} \quad (4)$$

where c is velocity of light in vacuum [6]. Work is in progress to improve this resolution by the application of a separation algorithm of superposed pulse echoes based on a linear optimization technique. On the other hand, the thickness precision is determined by variation of optical pass length of probe pulse and/or THz pulse caused by air disturbance or mechanical vibration. For example, when the path length fluctuates within ±10 μm due to those disturbances, a peak position of THz echo pulse deviates within ±33 fs; this leads to thickness precision of 2.3 μm. A 1D distribution of the paint thickness in position range of 1–4 mm along X axis of the sample in Fig. 5(c) was determined to be 162 ± 21 μm ((mean) ± (standard deviation)) by the time separation between the two THz echoes, which is consistent with that measured by the contact-type thickness meter (175 μm). At the boundary between the unpainted and painted areas, a mixture of one and two echoes is observed (Fig. 5(b)). We consider that a blurring of edge at the boundary between the two areas is mainly due to insufficient transverse resolution rather than aberration or diffraction. In this way, the temporal evolution of the 2D THz tomography is clearly visualized as the illuminating position of the THz beam moves across the sample. Although the proposed system is applied to a single-layer paint film in this demonstration, it can be also extended to multilayer paint films. In this case, an ability to distinguish a paint boundary depends on a relationship between Fresnel reflection in paint film and signal-to-noise ratio in addition to the d_{min} value. Here, we consider a THz pulse echo from a paint boundary in two-layer paint film, in which the second-layer paint film with a group refractive index (n_{g2}) is layered on the first-layer paint film (white alkyd, $n_{g1} = 2.14$) as shown in an inset of Fig. 6. The n_{g2} value is selected within a range of 1.5–3.6 because group refractive indices of car body paints vary widely within 1.5–3.6 in THz region [6]. Fig. 6 shows a relationship between the n_{g2} value and ratio of the pulse echo to the incident pulse, which is calculated from Fresnel formula. Here, negative sign of the ratio indicates inverse of polarity in the pulse echo. From this relationship and a signal-to-noise ratio of 80, the present system can detect the paint boundary with difference of group refractive index up to 0.08 when THz absorption in paint films is negligible.

The remote sensing characteristics of the measurement mean that the THz paintmeter can monitor paint thickness even for wet paint for which conventional contact-type
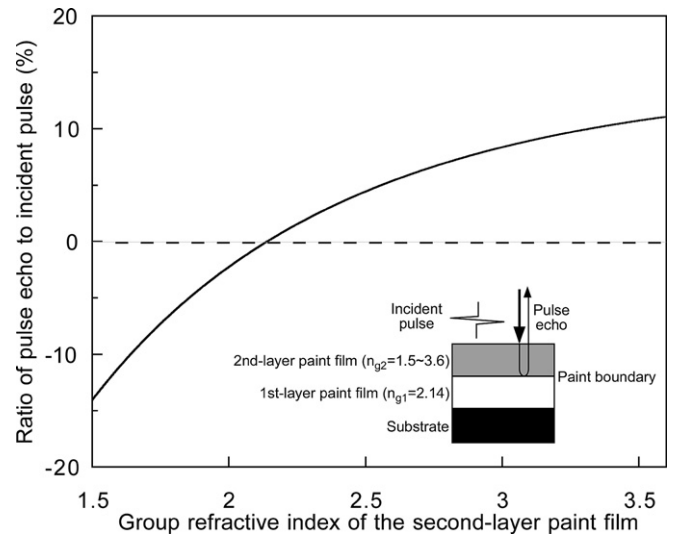

Fig. 6. Relationship between group refractive index of the second-layer paint film and ratio of pulse echo at paint boundary to incident pulse. Sample of two-layer paint film used in this calculation is illustrated as an inset.

thickness meters cannot be applied [6]. We here applied real-time 2D THz tomography to the monitoring of the drying progress of a wet paint film via the temporal change of the paint thickness during the wet-to-dry transformation. For this examination, an alkyd painting was made on an Al substrate just before the start of the measurement. A THz tomographic movie of the drying process in the wet paint film was measured over 20 min just after painting (see Movie 2). Fig. 7 shows snapshots of the THz tomographic movie at 1 min steps ($\theta = 20°$, image size = 6 ps × 5 mm), indicating that two THz echo signals temporally evolve over the period of the measurement. The left echo line (time = t_L) comes from the paint surface and hence relates to the geometric thickness of the paint film. Since the right echo line (time = t_R) is a reflection from the paint-substrate interface, time separation between the left and the right echo lines (time = $t_R - t_L = \Delta t$) relates to the optical thickness of the paint film. We determined the t_R and t_L values by averaging time values of two echo peaks along the vertical coordinate in Fig. 7, respectively, and then calculated the Δt values from them. Fig. 8 shows the evolution of the t_L and Δt values with respect to elapsed time, which indicating geometrical and optical shrinkage of the paint film during the wet-to-dry transformation. The solvent volatilization, triggering the wet-to-dry transformation, causes increase of the n_g value (see Fig. 4(b)) and the geometrical shrinkage (t_L in Fig. 8) in the wet paint film with drying progress. From comparison of temporal change between the t_L and Δt values, we can conclude that the optical shrinkage is dominated by the geometrical shrinkage. At 10 min, the temporal change was almost finished because of the quick-drying paint, implying completion of the drying process. It is also seen from Movie 2 and Fig. 7 that the shrinkage progresses uniformly in-plane. The data shown in Fig. 8 looks very similar to that shown in the previous
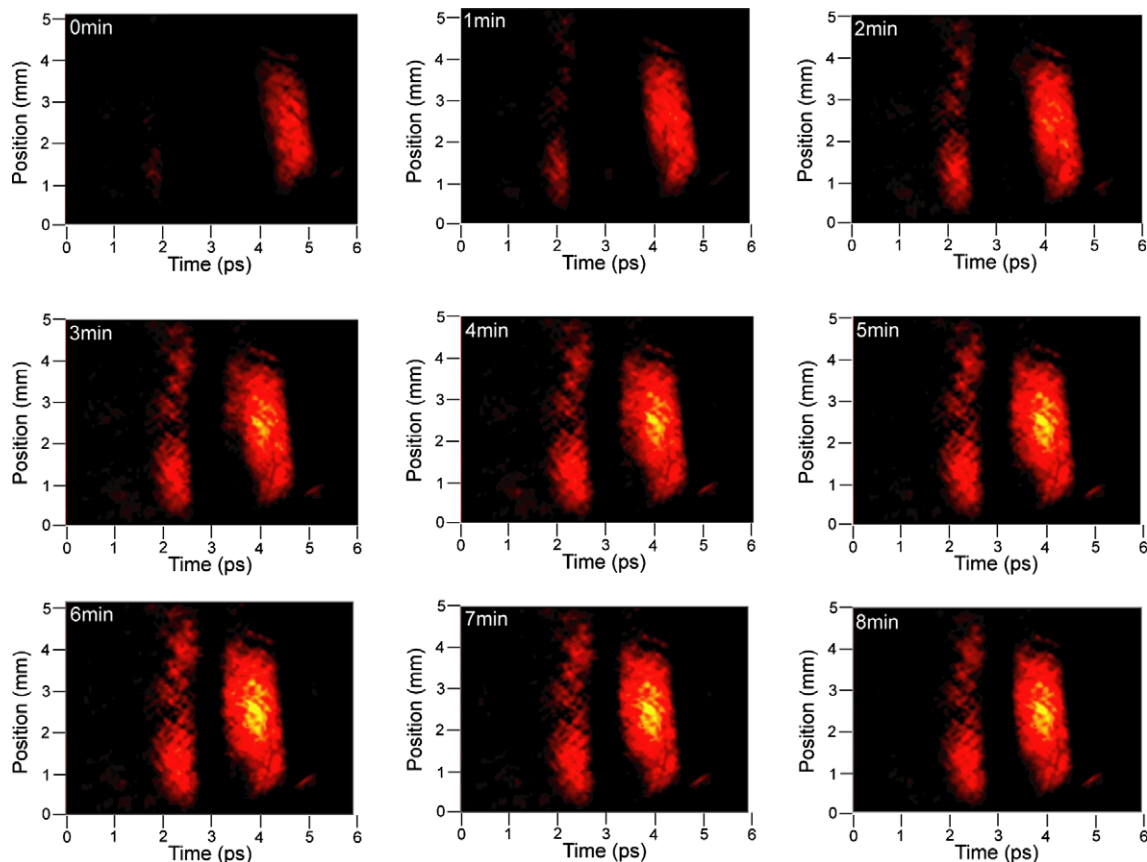
Fig. 7. 2D THz tomography of the drying process in the wet paint film at 1 min step ($\theta = 20°$, image size = 6 ps × 5 mm).
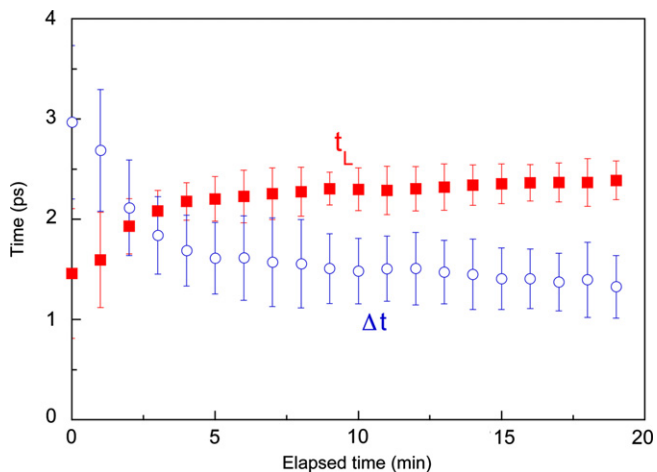

Fig. 8. Temporal change of t_L (left THz echo) and Δt values (time separation between the left and right echoes) with respect to elapsed time.

paper done with an oscillator-based THz paintmeter [6]. Such the similar results obtained from the two different methods indicate that the proposed method can monitor the drying progress correctly, because the two methods measure the same phenomena with respect to drying process. A little difference of convergence time between them is due to difference of drying speed between acryl paint and alkyd one. With respect to system cost, the proposed amplifier-based THz paintmeter is a few times more expen-sive than the previous oscillator-based one. However, the proposed system enables high-speed data acquisition attractive for practical applications. For example, a frame rate of 10 frame/s and an image size of 640×480 pixels in the present system provide nearly 3 Mpixels/s, which is already 480 times faster than the oscillator-based system in combination with a 10-Hz optical delay line. Such high-speed data acquisition opens the door to real-time 2D THz tomography of moving objects in *real world* and, more specifically, an in-process THz paintmeter.

4. Conclusions

We have proposed real-time 2D THz tomography based on the combined use of non-collinear 2D-FSEOS and line focusing of the THz beam on a sample. 2D spatiotemporal THz images are acquired at a frame rate of 10 frame/s and then used to visualize a 2D cross-section of the sample. We have demonstrated real-time monitoring of paint thickness in a moving paint sample and the drying dynamics in a wet paint film as examples of its application in a THz paintme-ter. To the best of our knowledge, this is the first time that 2D THz tomography of a moving object has been achieved in real time. This method will be useful in monitoring and/ or controlling industrial products on paint coating line and similar applications.

Acknowledgements

Appendix A. Supplementary data

Supplementary data associated with this article can be found in the online version, at doi:10.1016/j.optcom. 2006.05.063.

References

[1] D.M. Mittleman, R.H. Jacobsen, M.C. Nuss, IEEE J. Sel. Top. in Quantum Electron. 2 (1996) 679.
[2] D.M. Mittleman, S. Hunsche, L. Boivin, M.C. Nuss, Opt. Lett. 22 (1997) 904.
[3] A.J. Fitzgerald, B.E. Cole, P.F. Taday, J. Pharm. Sci. 94 (2005) 177.
[4] R.M. Woodward, B.E. Cole, V.P. Wallace, R.J. Pye, D.D. Arnone, E.H. Linfield, M. Pepper, Phys. Med. Biol. 47 (2002) 3853.
[5] D. Huang, E.A. Swanson, C.P. Lin, J.S. Schuman, W.G. Stinson, W. Chang, M.R. Hee, T. Flotte, K. Gregory, C.A. Puliafito, J.G. Fujimoto, Science 254 (1991) 1178.
[6] T. Yasui, T. Yasuda, K. Sawanaka, T. Araki, Appl. Opt. 44 (2005) 6849.
[7] L. Nicolaides, A. Mandelis, Opt. Express 7 (2000) 519.
[8] E. Bordenave, E. Abraham, G. Jonusauskas, J. Oberle, C. Rulliere, Opt. Express 10 (2002) 35.
[9] Q. Wu, T.D. Hewitt, X.-C. Zhang, Appl. Phys. Lett. 69 (1996) 1026.
[10] Z. Jiang, X.-C. Zhang, Appl. Phys. Lett. 72 (1998) 1945.
[11] Z. Jiang, X.-C. Zhang, Opt. Lett. 23 (1998) 1114.
[12] F.G. Sun, Z. Jiang, X.-C. Zhang, Appl. Phys. Lett. 73 (1998) 2233.
[13] S.P. Jamison, J. Shen, A.M. MacLeod, W.A. Gillespie, D.A. Jaroszynski, Opt. Lett. 28 (2003) 1710.
[14] Z. Jiang, F.G. Sun, X.-C. Zhang, Opt. Lett. 24 (1999) 1245.
[15] J. Shan, A.S. Weling, E. Knoesel, L. Bartels, M. Bonn, A. Nahata, G.A. Reider, T.F. Heinz, Opt. Lett. 25 (2000) 426.
[16] Z. Jiang, F.G. Sun, Q. Chen, X.-C. Zhang, Appl. Phys. Lett. 74 (1999) 1191.
[17] R. Rungsawang, A. Mochiduki, S. Ookuma, T. Hattori, Jpn. J. Appl. Phys. 44 (2005) L288.
[18] T. Yasui, T. Araki, Jpn. J. Appl. Phys. 44 (2005) 1777.